



# Molecular dynamics simulations of energy accommodation between gases and polymers for ultra-low thermal conductivity insulation

Tianli Feng\*, Amit Rai, Diana Hun, Som S Shrestha\*

Buildings and Transportation Science Division, Oak Ridge National Laboratory, Oak Ridge, Tennessee 37831, USA

## ARTICLE INFO

### Article history:

Received 18 May 2020

Revised 27 August 2020

Accepted 12 September 2020

Available online 8 October 2020

### Keywords:

Accommodation coefficient  
Gaseous thermal conductivity  
Amorphous polymers  
Molecular dynamics  
Thermal insulation materials

## ABSTRACT

Determining the energy accommodation between gases and solids is essential to developing porous thermal insulation materials with ultra-low effective thermal conductivity that reduce energy use, greenhouse gas emissions, and fossil fuel consumption. The energy accommodation coefficients of most gases, however, have been rarely studied, especially with respect to solids that have relatively high thermal resistivity, e.g., polymers. In this work, by using all-atom nonequilibrium molecular dynamics simulations, we reveal the accommodation coefficients of He, Ar, N<sub>2</sub>, and O<sub>2</sub> with polymers, mainly polystyrene. We find that their values are around 0.51, 0.72, 0.79, and 0.90, respectively, suggesting a critical reexamination of the commonly used theoretical maximum value of 1. We have also conducted experiments and validated the value for air, which is about 0.81. Such a change in accommodation coefficients can lead to a reduction of about 70%, 50%, 35%, and 20% in the thermal conductivity of He, Ar, N<sub>2</sub>, and O<sub>2</sub> gases in nano pores (below 100 nm) or at low pressures (below 1 millibar). With these new accommodation coefficients, we find that in a 10 nm pore with ambient pressure at 300 K, the gas thermal conductivity of He, Ar, N<sub>2</sub>, and O<sub>2</sub> in porous polystyrene can be as low as  $9.7 \times 10^{-4}$ ,  $3.4 \times 10^{-4}$ ,  $7.3 \times 10^{-4}$ , and  $8.5 \times 10^{-4}$  W·m<sup>-1</sup>·K<sup>-1</sup>, respectively, which are two to three orders of magnitude lower than their bulk values, promising higher thermal resistivity of insulation materials. This work reveals the fundamental energy exchange between gases and polymers, providing important guidance for designing high-performance thermal insulation materials for various applications.

© 2020 Elsevier Ltd. All rights reserved.

## 1. Introduction

Developing thermal insulation materials with ultra-low effective thermal conductivity is of significant interest in many applications such as oil transportation, aerospace engineering, and building envelopes, to reduce energy use, greenhouse gas emissions, and fossil fuel consumption [1, 2]. For example, as the largest energy consumption sector, buildings use about 40% of the overall primary energy in the United States [3] and the European Union [4]. Of the various factors that affect building energy use, heating and air-conditioning are the greatest contributors [5]. Therefore, the development of high performing thermal insulation materials that decrease heat transfer through building envelopes is essential to reduce heating and cooling loads.

Significant efforts have been made to reduce the thermal conductivity of materials, which typically use micro- or nano-porous structures, as well as low thermal conductivity gases and/or re-

duced pressure inside the pores [6–10]. In these materials, gaseous thermal conductivity is usually the major contributor to thermal transport, while the roles of solid conduction and radiation are relatively small [2]. Therefore, the key to improving the thermal resistance of porous insulation materials is to reduce the thermal energy transport through gases, which often requires the porous structure to have pore sizes smaller than the mean free path of the gas molecules [2]. Under these circumstances, gas thermal conductivity reaches the subcontinuum regime and exhibits strong dependence on the pore size, gas pressure, and the energy exchange efficiency between gases and solid surfaces, i.e., the energy accommodation coefficient,  $\alpha$  [11–13].

Determining the energy accommodation coefficients between gases and solids are a key part to understanding and reducing the effective thermal conductivity of thermal insulation materials [14, 15]. The value of the accommodation coefficient varies from 0 to 1, with 0 representing no energy exchange and 1 representing maximum energy exchange efficiency between the gas and the solid surface in their collisions. Extensive efforts have focused on solid/solid interfacial resistances [16, 17] as well as accommoda-

\* Corresponding authors.

E-mail addresses: [fengt@ornl.gov](mailto:fengt@ornl.gov) (T. Feng), [shresthass@ornl.gov](mailto:shresthass@ornl.gov) (S.S. Shrestha).

tion coefficients between gases and hard (inorganic) materials surfaces such as semiconductors [18, 19], metals [20–23], carbon nanotubes [24], or graphene [24, 25]. Due to measurement and simulation difficulties, the study of the interface between gases and soft materials, e.g., amorphous polymers, has received minimal attention. Considering that the accommodation coefficient increases with increasing surface roughness [26, 27], for simplicity, many studies assumed a perfect accommodation [28–31], i.e.,  $\alpha = 1$ , or some other plausible values [32, 33] when studying thermal insulation materials. The need to establish a database of the accommodation coefficients of various gases has long been known to be essential to developing thermal insulation materials with ultra-low effective thermal conductivity [18, 34]. To reveal the theoretical accommodation coefficients between various gases and polymers, we perform nonequilibrium molecular dynamics (NEMD) simulations using all-atom interatomic potentials.

The remainder of this manuscript is organized as follows. In Sec. 2, we describe the methodology to calculate the energy accommodation coefficient by NEMD simulations, material structures, and NEMD simulation setups. In Sec. 3, we briefly discuss the establishment of interatomic potentials between polymer atoms and gas atoms since the interaction between polymers and gases has been minimally studied. In Sec. 4, the accommodation coefficients of He, Ar, N<sub>2</sub>, and O<sub>2</sub> are estimated and compared with the literature. In Sec. 5, the gas thermal conductivities of He, Ar, N<sub>2</sub>, and O<sub>2</sub> as functions of pore diameter and pressure are evaluated and compared with those obtained from perfect accommodation. In Sec. 6, we compare our MD simulation results with our experimental data. In Sec. 7, we examined the impact of gas pressure, pore diameter, and the gas accommodation coefficient on the thermal conductivity of gases. In Sec. 8, conclusions are presented.

## 2. Materials and methods

The energy accommodation coefficients,  $\alpha$ , of gas molecules on polymer surfaces are calculated based on the relationship between  $\alpha$  and the polymer/gas interfacial thermal conductance  $G_{int}$  [35]:

$$G_{int} = 4k_B N \cdot \frac{\alpha}{2 - \alpha}. \quad (1)$$

$k_B$  is the Boltzmann constant.  $N$  is the collision rate of gas molecules on polymer surfaces per unit area given by

$$N = \frac{n}{4} \sqrt{\frac{8k_B T}{\pi m}} \quad (2)$$

or

$$N = \frac{P}{\sqrt{2\pi m k_B T}}, \quad (3)$$

where  $n$  is the number density of gas molecules,  $T$  is the temperature,  $P$  is the pressure, and  $m$  is the molar mass of gas molecules. Note that although Eq. (1) is usually used with flat interfaces, it can also be applied to rough interfaces such as with polymers [15] as long as we set an imaginary plane as the interface. An imaginary plane at the position that is an interatomic potential cutoff distance (10 Å in this work) away from the solid surface is set as the solid/gas interface to calculate the interfacial resistance [15, 27, 36]. The incident (or reflected) gas atoms passing through the imaginary plane indicate the start (or finish) of the energy exchange process. In this work, since the surface of the polymer is rough as shown in Fig. 1, we find the average position of the surface and set the imaginary plane 10 Å away from this average position. Because the position of the imaginary plane adds uncertainty to the results, we move the imaginary plane by  $\pm 10$  Å to account for such uncertainty and represent its effects on the accommodation factor results later on. To calculate the collision rate of the

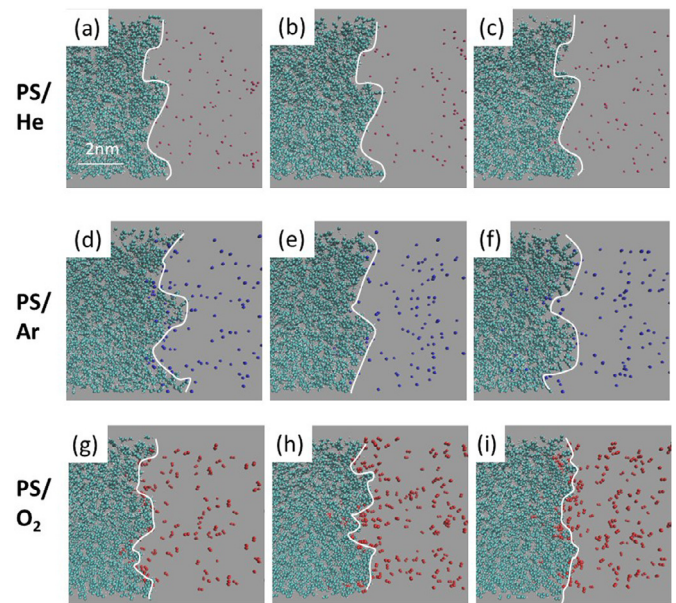


Fig. 1. Snapshots of the surface region of (a-c) PS/He, (d-f) PS/Ar, and (g-i) PS/O<sub>2</sub> interfaces during the NEMD simulations. The snapshots of each system are taken within 1 ns. The surface profiles are depicted using white lines.

gas molecules, we tried both Eq. (2) and (3) and found that they give similar results. Therefore, we average their results to calculate the collision rate and minimize statistical error. We calculate the polymer/gas interfacial thermal conductance,  $G_{int}$ , via NEMD simulations that we perform using the Large-scale Atomic/Molecular Massively Parallel Simulator (LAMMPS) [37].

The gases we study include the noble gases He and Ar, as well as the commonly used gases in thermal insulation materials, N<sub>2</sub> and O<sub>2</sub>. We also briefly consider CO<sub>2</sub>. We selected He and Ar because they have been extensively studied with other solid surfaces [18–25] and they are monatomic gases with simple potential forms, which are best choices for benchmarking. We selected N<sub>2</sub>, O<sub>2</sub>, and CO<sub>2</sub> because they are components of air that fill the pores in common polymeric thermal insulation materials. Amorphous polystyrene (a-PS), with chemical formula (C<sub>8</sub>H<sub>8</sub>)<sub>n</sub>, is the selected polymer because it is a commercial thermal insulation material used in buildings. We expect the results to be roughly applicable to other polymers composed of C and H since theoretically the accommodation coefficients are determined by the van der Waals interaction between the polymer's C/H atoms and the gas molecules, and this van der Waals interaction is the same for most polymers, i.e., it does not depend on whether the C/H atoms belong to -CH<sub>3</sub>, -CH<sub>2</sub>-, -CH=, or -C<sub>6</sub>H<sub>5</sub> [38]. To further examine this assumption, we repeated the simulations on the He/amorphous polyethylene (C<sub>2</sub>H<sub>4</sub>)<sub>n</sub> system and found similar results to the He/a-PS system. Nevertheless, we do not exclude the possibility that some polymers with very different chemical components may have different accommodation coefficients.

The polymer structures and polymer consistent force field (PCFF) are obtained via Material Studio [38] by Monte Carlo energy minimization simulations. The cutoff radii of Lennard-Jones (LJ) and electrostatic potential are set as 10 and 9.5 Å, respectively. Ewald summation is used to account for the electrostatic potential beyond the cutoff radius. The time step of MD simulations is 1 fs.

The pore or cell and gas layout that was used in the NEMD simulation is shown in Fig. 2. Periodic boundary conditions are applied along all three dimensions. Two identical 7-nm thick polymer blocks are set as the heat source and sink, located at  $\frac{1}{4}$  and  $\frac{3}{4}$  of the overall NEMD domain, with temperatures of  $T_1$  and  $T_2$ , respec-

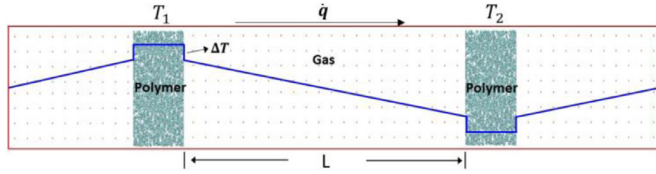


**Fig. 2.** Schematic of the NEMD simulation domain and setups to calculate the polymer/gas thermal accommodation coefficient. Polymer blocks are set as heat reservoirs. Periodic boundary conditions are applied along all three dimensions. Dimensions are not drawn to scale. The blue lines illustrate the temperature profile.

tively. The remaining space is filled by gas molecules, which forms two blocks as well (note that the left and right blocks belong to one single block due to the periodic boundary condition). Each a-PS block is composed of six atactic PS chains with 70 PS monomers per chain and measures  $72 \times 36 \times 36 \text{ \AA}^3$  in size, with the longer length aligned along the heat transport direction to prevent the gas molecules from penetrating through the polymer blocks. Each polymer block contains 6732 atoms, and each gas block contains 828 molecules. We tried different number of gas molecules, pressures, and box lengths for helium in a convergence study, and the obtained accommodation coefficient values are consistent. Therefore, for all the other gases, to mitigate the computational cost (similar to Ref. [15, 24]), we choose a high gas pressure,  $\sim 30$  bar, which leads to the length of each gas block,  $L$ , being about  $1100 \text{ \AA}$ .

Note that using a fixed boundary condition along the heat flux direction can reduce the domain size and computational cost. Nevertheless, we choose a periodic boundary condition because we found that it must be used to avoid possible bond breaking or atom loss during the MD simulations due to the polymer structures and potential format outputted from Material Studio. In the NEMD simulations in the literature, periodic boundary conduction in the heat flux direction is commonly seen, in which the  $1/4 L$  location is set as a heat source and the  $3/4 L$  location is set as a heat sink [39–42]. The use of periodic or fixed boundary conduction are both commonly seen in the literature and this choice will not affect the results, especially in cases in which we primarily care about the interfacial heat flux and interfacial temperature jump  $\Delta T$ .

Four polymer/gas interfaces, i.e., on both sides of the heat source and heat sink, are formed in the simulation cells. To simulate the gas accommodation coefficient at 300 K, two options for the temperature setup can be used. One option is to set the heat source at 300 K and the heat sink at a different temperature, so that the accommodation coefficient can be estimated based on the two surfaces of the heat source. The other option is to set the heat source and sink at  $T_1 = 330 \text{ K}$  and  $T_2 = 270 \text{ K}$ , respectively. The accommodation coefficient is then obtained by averaging the four surfaces. To minimize the statistical error, we use the second option since it has four interfaces per simulation.

The systems are first relaxed in the NVT (constant mass, volume, and temperature) ensemble for 1 million steps and then switched to the NVE (constant mass, volume, and energy) ensemble with fixed temperatures being applied to the polymer reservoirs. The reservoirs can usually be modulated by the Langevin or Berendsen thermostat. We choose the Berendsen thermostat since we find that the Langevin thermostat converges slowly in the polymer/gas systems. Under the NVE ensemble, the simulations are run until the heat flux and temperature profile of the systems reach steady state. The surface morphology varies with time, as seen in Fig. 1. Due to these changes in morphology and the low thermal conductivity of the systems, the simulations often require a considerable amount of time, i.e., 6–31 million steps (6–31 ns), to reach steady state. Each system is simulated three to five times to minimize the statistical error of MD. With the NEMD simulations, the

**Table 1**

Parameters of the 9-6 LJ potential for the van der Waals interaction within a-PS built in the PCFF potential via Material Studio [38]. Other polymers composed of C and H, such as polyethylene and polypropylene, have the same values. The PCFF potential also includes bond-order and electrostatic potentials, which are not shown here.

Polymer elements Comments	C On phenyl rings	C Other	H
$\epsilon_1$ (meV)	2.775	2.342	0.867
$\sigma_1$ (Å)	4.01	4.01	2.995

**Table 2**

Parameters of the 12-6 LJ potential for van der Waals inter-molecular interactions of gases. Parameters of He and Ar are taken from Ref. [45]. Parameters of  $N_2$  and  $O_2$  are taken from Ref. [46].

Gases	He	Ar	$N_2$	$O_2$
$\epsilon_2$ (meV)	0.88	10.61	3.21	5.31
$\sigma_2$ (Å)	2.56	3.40	3.31	2.95

polymer/gas interfacial thermal conductance  $G_{int}$  is calculated by

$$G_{int} = \frac{\dot{q}}{\Delta T \cdot A} \quad (4)$$

where  $\dot{q}$  is the heat flux flow rate,  $\Delta T$  is the temperature drop at the interface, and  $A$  is the cross-sectional area.

### 3. Lennard-Jones potentials between polymer and gases

The interactions between polymer atoms, i.e., C and H, are described by the PCFF potential that is optimized via Material Studio [38], which includes the combination of bond-order potentials, electrostatic interaction, and a 9-6 Lennard-Jones (LJ) potential. These potentials are well established [38], hence we only discuss the last term, i.e., the 9-6 LJ term,

$$V_{9-6} = \epsilon_1 \left[ 2 \left( \frac{\sigma_1}{r} \right)^9 - 3 \left( \frac{\sigma_1}{r} \right)^6 \right] \quad (5)$$

because it will be used to establish the interaction between the polymer and gases.  $\epsilon_1$  is a parameter representing the interaction strength.  $\sigma_1$  determines the equilibrium distance among atoms.  $r$  is the interatomic distance. Values for  $\epsilon_1$  and  $\sigma_1$  are listed in Table 1. The intermolecular interaction of gases is described by the 12-6 LJ potential:

$$V_{12-6} = 4\epsilon_2 \left[ \left( \frac{\sigma_2}{r} \right)^{12} - \left( \frac{\sigma_2}{r} \right)^6 \right] \quad (6)$$

where the values of  $\epsilon_2$  and  $\sigma_2$  for He, Ar,  $N_2$  and  $O_2$  are listed in Table 2. An intramolecular potential is also needed for  $N_2$  and  $O_2$ , which are diatomic molecules. Based on Ref. [43],  $O_2$  is described by a harmonic bond  $V_{O-O} = \frac{k_b}{2} (b - b_0)^2$ , with bond length  $b_0 = 1.21 \text{ \AA}$  and bond energy  $k_b = 4000 \text{ kJ} \cdot \text{mol}^{-1} \cdot \text{\AA}^{-1}$ .  $N_2$  is described by rigid bonds with bond length of  $1.09 \text{ \AA}$  [44].

To describe the interaction between polymers and gas molecules, usually the mixing rules  $V_{ij} = 4\epsilon^{ij} \left[ \left( \frac{\sigma^{ij}}{r} \right)^{12} - \left( \frac{\sigma^{ij}}{r} \right)^6 \right]$  with  $\epsilon^{ij} = \sqrt{\epsilon^i \epsilon^j}$  and  $\sigma^{ij} = (\sigma^i + \sigma^j)/2$  can be used if the intra-solid and intra-gas interactions are described by the 12-6 LJ potentials  $V_{ii} = 4\epsilon^{ii} \left[ \left( \frac{\sigma^{ii}}{r} \right)^{12} - \left( \frac{\sigma^{ii}}{r} \right)^6 \right]$  and  $V_{jj} = 4\epsilon^{jj} \left[ \left( \frac{\sigma^{jj}}{r} \right)^{12} - \left( \frac{\sigma^{jj}}{r} \right)^6 \right]$ , respectively. Here,  $i$  and  $j$  represent the atoms of the solid and gas, respectively, and  $r$  is the interatomic distance. This method has been successfully used in many systems such as noble gases and carbon nanotubes [24]. To apply the mixing rule to polymer/gas systems, we need to approximate the 9-6 LJ parameters  $\epsilon_1$  and  $\sigma_1$

**Table 3**  
Parameters of the 12-6 LJ potential for van der Waals interactions between polymer atoms and gas atoms.

Gas elements	$\epsilon_2$ (meV)			$\sigma_2$ (Å)		
	Polymer elements					
	C (phenyl rings)	C (other)	H	C (phenyl rings)	C (other)	H
He	1.353	1.243	0.757	3.064	3.064	2.613
Ar	4.699	4.317	2.627	3.484	3.484	3.033
N	2.585	2.375	1.445	3.439	3.439	2.988
O	3.324	3.054	1.858	3.259	3.259	2.808

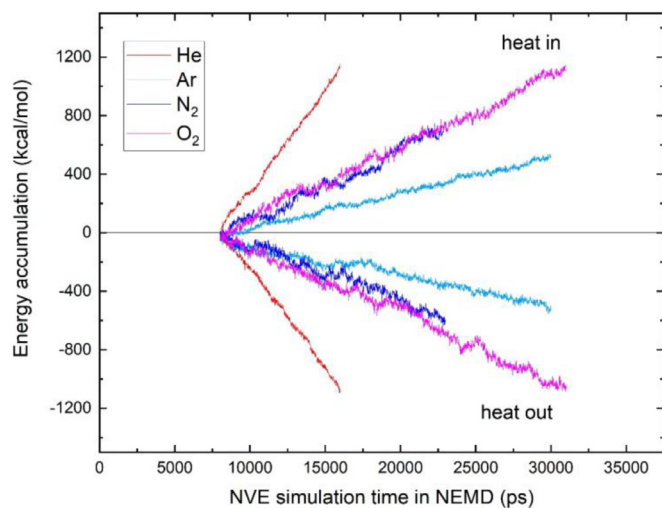


**Fig. 3.** Energy accumulations in the hot and cold reservoirs in the polystyrene/gas systems after the systems are turned into an NVE ensemble with thermal reservoirs applied. Data from the first 8 ns of the NVE simulations are not shown because the systems had not stabilized.

of the polymers to be 12-6 LJ parameters  $\epsilon_2$  and  $\sigma_2$ . The approximation needs to ensure that the equilibrium interatomic distance  $r_m$  and the force at the equilibrium interatomic distance  $\frac{\partial^2 V}{\partial r^2}|_{r_m}$  are consistent. Considering  $r_m = \sigma_1$  and  $\frac{\partial^2 V}{\partial r^2}|_{r_m} = \frac{54}{\sigma_1^2}\epsilon_1$  for 9-6 LJ potentials and  $r_m = 2^{1/6}\sigma_2$  and  $\frac{\partial^2 V}{\partial r^2}|_{r_m} = \frac{72}{2^{1/3}\sigma_2^2}\epsilon_2$  for 12-6 LJ potentials, we calculate that  $\sigma_2 = 2^{-1/6}\sigma_1 \approx 0.89\sigma_1$  and  $\epsilon_2 = \frac{3}{4}\epsilon_1$ . Therefore, with the mixing rule, the 12-6 LJ potential parameters between polymer atoms and gas atoms are calculated as shown in Table 3.

#### 4. Energy accommodation coefficients of gases

To estimate the gas energy accommodation coefficients,  $\alpha$ , through Eq. (1), we calculate the interfacial thermal conductance  $G_{int}$  using Eq. (4) and NEMD simulations. The heat flow rates  $\dot{q}$  through the systems are obtained by the time derivatives of the energy accumulation in the thermal reservoirs (polymer blocks shown in Fig. 2). The energy accumulations as a function of time for the various systems are shown in Fig. 3. A challenge is that the systems usually require long simulations to reach steady state due to their low thermal conductivity. Consequently, in Fig. 3 we omit data from 0 to 8 ns after the two heat reservoirs are applied to the systems because the heat flows are unsteady. After 8 ns, the systems reach steady state at different times depending on the gas. When the studied gases are exposed to the same conditions, He has the highest thermal conductivity and we use 16 ns to estimate the heat flow rate through the polymer/He system. For the other gases, 24–31 ns is used to get reliable heat flow rate data.

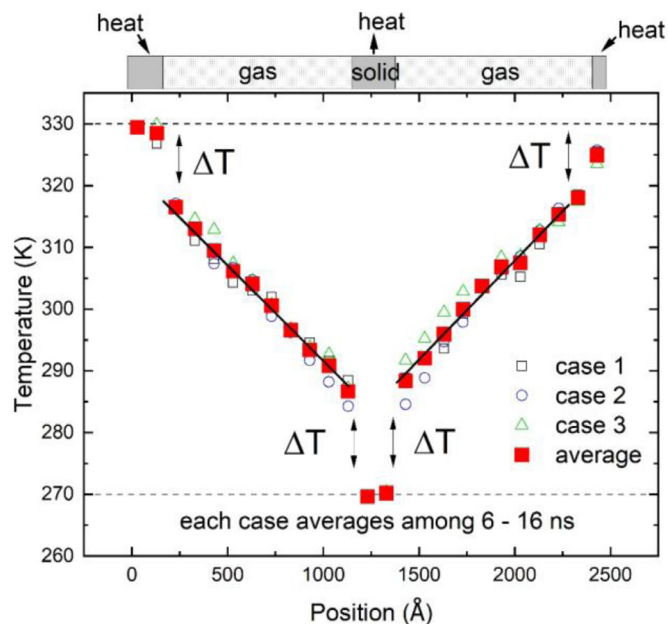


**Fig. 4.** Temperature profiles of the a-PS/He (g) system. The dashed lines are the temperatures of the heat reservoirs (330 K for hot and 270 K for cold). The schematic at the top is essentially the same as Fig. 2, and the polymer blocks at the left and right ends belong to a single polymer block, i.e. hot reservoir, considering that periodic boundary condition is used. Three independent simulations are performed, and their average is used to calculate the temperature gradient and jumps.

An example temperature profile is given in Fig. 4, showing a clear temperature jumps at the polymer/gas interfaces. The value of  $\Delta T$  is taken as an average among the four interfaces of three independent simulations. With  $\dot{q}$  and  $\Delta T$ , the interfacial resistance  $G_{int}$  is calculated using Eq. (4), and the accommodation coefficient  $\alpha$  is obtained using Eq. (1).

The accommodation coefficients  $\alpha$  of He, Ar,  $N_2$ , and  $O_2$  are found to be 0.51, 0.66, 0.79, and 0.90, respectively, as shown in Table 4. The  $\alpha$  value for air can be approximated as 0.81, considering 79%  $N_2$ , 21%  $O_2$ , and 1% Ar. The  $\alpha$  values of various gases are generally positively correlated with the bonding strengths,  $\epsilon_2$  in Table 3, between gas and polymer atoms, which is understandable as  $\alpha$  is a measurement of the energy exchange efficiency between the gas and the solid surface. Note that although the  $\epsilon_2$  values of  $N_2$  and  $O_2$  atoms are smaller than that of Ar according to Table 3, the diatomic nature of  $N_2$  and  $O_2$  can roughly double the interaction strength, making the accommodation coefficient of  $N_2$  and  $O_2$  larger. Our results provide a critical reexamination of the typical assumption that the gas accommodation coefficient with polymers is the theoretically maximum value of 1 due to rough surfaces [28–31]. Actually, it has been found that the interaction time between gas and polymeric surfaces does not increase by increasing the surface roughness as long as  $\epsilon$  is smaller than 10 meV [15].

**Table 4**

Energy accommodation coefficients  $\alpha$  of He, Ar, N<sub>2</sub>, and O<sub>2</sub> on a-PS at 300 K calculated in this work, as well as measured and simulated  $\alpha$  values from the literature for other solid surfaces.

	Solid surface	Ref.	He	Ar	N <sub>2</sub>	O <sub>2</sub>
MD (This work)	a-PS		0.51 ± 0.04	0.72 ± 0.05	0.79 ± 0.06	0.90 ± 0.1
Metals	Stainless steel, Au, Al, Pt, Si, Si <sub>3</sub> N <sub>4</sub>	[26]	0.35-0.45	0.87-0.95	0.8-0.85	-
(Exp.)	Au, Pt	[50]	-	0.71, 0.78	-	-
Lit.)	W, Pt, Al, Be, K, Na	[21, 47] Review	0.017-0.145	0.3	-	-
Rough	Fused silica	[48]	-	-	0.84 (air)	-
(Exp.)	poly(dimethyl-diallyl-ammonium) chloride	[48]	-	-	0.92 (air)	-
MD	Pt, Au	[15, 20]	-	0.44, 0.58	-	-
(Lit.)	Graphene	[24]	0.2	0.9	-	-
	Self-assembled monolayers	[15]	-	0.97	-	-

Because no experimental data on the  $\alpha$  between gases and polystyrene, polyethylene or other C-H-polymers, are available in the literature, we conducted experiments to validate our predictions as explained in a following section. Before that, we compare our results with the available experimental  $\alpha$  for available materials, as shown in Table 4, for possible insights. There are large discrepancies in the  $\alpha$  values from experimental work described in the literature. For example, based on a review by Wachman [47], the most reliable  $\alpha$  values of He on many metals, including tungsten (W), platinum (Pt), aluminum (Al), beryllium (Be), Potassium (K), and sodium (Na), are as low as 0.017–0.145, while a recent measurement study [26] produced an  $\alpha$  value of about 0.35–0.45 for many metals and semiconductors. It is thought that  $\alpha$  values are sensitive to the measurement methods and surface conditions of solids [20, 26, 47]. Clean surfaces or higher temperatures usually give lower  $\alpha$  values due to the reduced adsorption of gas molecules on surfaces. In our work on polymers, we observed very little gas molecule adsorption as shown in Fig. 1. Nevertheless, for both organic solids from our simulations and inorganic solids from experiments in the literature,  $\alpha$  (Ar) is similar to  $\alpha$  (N<sub>2</sub>) and is much larger than  $\alpha$  (He). And, our results on C-H-polymers are similar to those measured from fused silica and poly (dimethyl-diallyl-ammonium) chloride, which also have rough surfaces [48]. In this regard, our simulation results are reasonable.

We also compare our simulation results on polymers with MD simulation results for other materials described in the literature. Generally, the trend that we observed in which  $\alpha$  increases with increasing  $\epsilon$  values for polymers is consistent with that found in gas/metal and gas/carbon nanotube systems [20, 24]. Liang *et al.* [15] found that Ar has an accommodation coefficient of about 1 on self-assembled monolayers, which is quite different from our results on polymers. We attribute this difference to the different simulation methods and potentials we used. Specifically, Liang *et al.* [15] use a coarse-grained potential to simulate a polymer in which the hydrocarbon groups (e.g., -CH<sub>3</sub>) are treated as single interaction sites, whereas we use all-atom simulations that explicitly consider the C-gas and H-gas interactions, which should give more reliable results. Nevertheless, we acknowledge that the accuracy of all simulations needs to be validated by future experimental efforts.

We also compare our results with the hard-sphere model [49],  $\alpha = 2.4\mu/(1 + \mu)^2$ , where  $\mu$  is the mass ratio between gas molecules and solid atoms. However, a difficulty is to approximate the mass of a “polystyrene atom”. If we take the average atomic mass ( $m_C + m_H$ )/2 = 6.5 g/mol as the mass of a “polystyrene atom”, the accommodation coefficient of He, Ar, N<sub>2</sub>, and O<sub>2</sub> are 0.57, 0.29, 0.52, and 0.49, respectively. Clearly, this estimation does not agree with our NEMD simulation results due to the following reasons: 1) the hard-sphere model only takes into account mass impact while ignoring the important impact of interatomic interaction strength, i.e., various gases have various interaction strengths with polymers; 2) the estimation of the mass of a “polystyrene atom” is not

reasonable since polystyrene is composed of -C<sub>6</sub>H<sub>5</sub> groups and -C<sub>2</sub>H<sub>2</sub>- units with covalent bonds and van der Waals interactions, rather than single atoms like in inorganic materials; 3) the hard-sphere model assumes the coarse-grain model for gas molecules, which can give a large error. For instance, we find that when the diatomic gas (O<sub>2</sub>) is treated as a single ball in the NEMD simulations, the calculated accommodation coefficient is much smaller than that given by all-atom simulations. Thus, we show the importance of conducting all-atom simulations for polymer/gas interfaces compared to a rough model that was developed for inorganic materials.

## 5. Subcontinuum thermal conductivity of gases

With the gas accommodation coefficient, we are able to evaluate the subcontinuum thermal conductivity of gases,  $\kappa_{gas}$ , under various conditions to guide the design of porous materials with different pore diameters ( $D$ ), porosities, and pressures. The widely used formula for  $\kappa_{gas}$  from Kaganer [51] is a function of the gas bulk thermal conductivity  $\kappa_{gas}^0$  at a given temperature, the gas molecules kinetic mean free path  $\Lambda$ , and a coefficient  $\beta$ ,

$$\kappa_{gas} = \kappa_{gas}^0 \frac{1}{1 + 2\beta \frac{\Lambda}{D}} \quad (7)$$

where  $\beta$  is a property of the gas that is determined by the gas accommodation coefficient  $\alpha$ , Prandtl number  $Pr$ , and the ratio of the specific heats  $\gamma = C_p/C_v$ ,

$$\beta = \frac{2\gamma}{\gamma + 1} \frac{1}{Pr} \frac{2 - \alpha}{\alpha} \quad (8)$$

and  $\Lambda$  is a function of temperature  $T$ , gas kinetic diameter  $d$ , and gas pressure  $P$ ,

$$\Lambda = \frac{k_B T}{\sqrt{2\pi} d^2 P} \quad (9)$$

Eq. (7) describes the change in thermal conductivity due to the change in the ratio of the mean free path to pore size ( $\Lambda/D$ ) together with the gas/solid interfacial resistance. In the diffusive regime, i.e., when the system size is much larger than the particle's mean free path, a change in pressure (particle density) does not affect the gas thermal conductivity. This is because an increase in particle density decreases the mean free path of particles, which offsets the increase in heat capacity (particle density) for thermal transport; therefore, thermal conductivity is independent of pressure. However, in the ballistic regime, i.e., when the particle mean free path is much larger than  $D$ , gas thermal conductivity decreases significantly with lower pressure because the heat capacity (particle density) also decreases with pressure, while the particle mean free path does not increase at the same rate due to the finite boundary ( $D$ ) confinement. Therefore, the gas thermal conductivity decreases with decreasing  $D$  or pressure, known as size effect, or subcontinuum thermal transport effect.

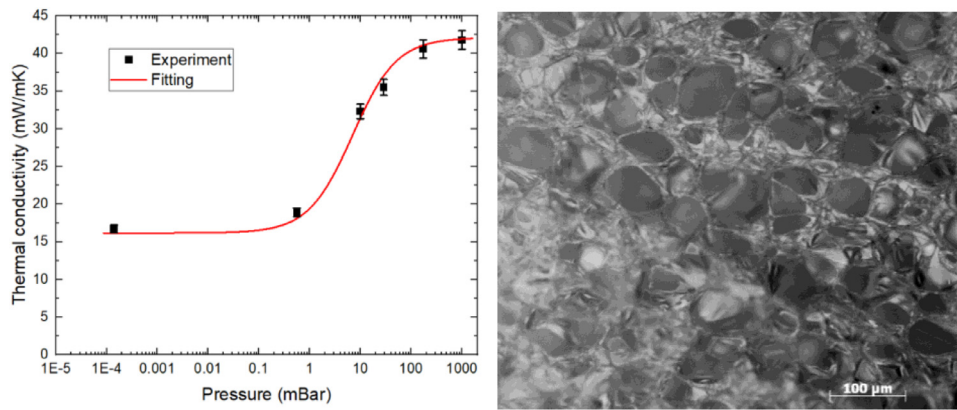


Fig. 5. Left: Thermal conductivity measurements from EPS and its fitting using Eq. (10). Right: SEM image of EPS sample.

Table 5

Gas parameters of He, Ar, N<sub>2</sub>, and O<sub>2</sub> at 300 K, including the factor  $\beta$  in Eq. (8), Prandtl number  $Pr$ , ratio of the specific heats  $\gamma = C_p/C_v$ , kinetic diameter  $d$ , and bulk thermal conductivity of gases  $\kappa_{gas}^0$  taken from the literature [52–55]. The  $\beta$  value of air can be approximated as  $\beta(\text{air}) = 2.44$ , considering 78% N<sub>2</sub>, 21% O<sub>2</sub> and 1% Ar.

	He	Ar	N <sub>2</sub>	O <sub>2</sub>
$\beta$	$5.61 \pm 0.55$	$3.41 \pm 0.41$	$2.55 \pm 0.30$	$2.00 \pm 0.36$
$Pr$	0.65	0.65	0.70	0.71
$\gamma$	1.66	1.66	1.40	1.40
$d$ (nm)	0.260	0.340	0.364	0.346
$\kappa_{gas}^0$ (W•m <sup>-1</sup> K <sup>-1</sup> )	0.151	0.018	0.026	0.027

At the maximum accommodation of  $\alpha = 1$ , the value of  $\beta$  is usually assumed to be around 1.5 to 2 in the literature, which is commonly used when the accommodation coefficient is unknown [28–31]. In the diffusive regime, i.e., the pore diameter  $D$  is much larger than  $\Lambda$ ,  $\kappa_{gas}$  is pressure independent, which results in the ‘bulk’ thermal conductivity  $\kappa_{gas}^0$ . The values of the previously mentioned parameters are listed in Table 5.

## 6. Validation against experiment

With Eq. (7), we can validate our MD simulation results with experimental data. The thermal conductivity of porous materials is composed of gas conductivity  $\kappa_{gas}$ , solid conductivity  $\kappa_{solid}$ , and radiative conductivity  $\kappa_{rad}$ . Solid and radiative thermal conductivities are independent of gas pressure and can be written as a constant. Therefore, the thermal conductivity of a porous material as a function of pressure can be written as

$$\kappa(P) = \kappa_{gas} + \kappa_{solid} + \kappa_{rad} = \kappa_{gas}^0 \frac{\phi^{2/3}}{1 + 2\beta \frac{k_B T}{\sqrt{2\pi} d^2 P}} + \text{Const} \quad (10)$$

where  $\phi$  is the porosity.  $\phi^{2/3}$  originates from the Russell model [59]. We measured the pressure-dependent thermal conductivity  $\kappa(P)$  of expanded polystyrene (EPS) with density of 0.0138 g/cm<sup>3</sup> and pores that were filled with air, while maintaining the temperature at 297 K. The measurements shown in Fig. 5 were used with Eq (10) to fit  $\beta/D$  and Const, giving  $\frac{\beta}{D} = 0.0489 \mu\text{m}^{-1}$ . To get the value of  $\beta$ , we determined the pore diameter  $D$  to be  $50 \pm 5 \mu\text{m}$  through an SEM image of the sample shown in Fig. 5. Afterwards,  $\beta$  was estimated as  $2.45 \pm 0.25$ , which matches well with our MD results shown in Table 5.

## 7. Ultra-low thermal conductivity insulation

In this work we mainly examine the impact of gas pressure, pore diameter, and the gas accommodation coefficient on the ther-

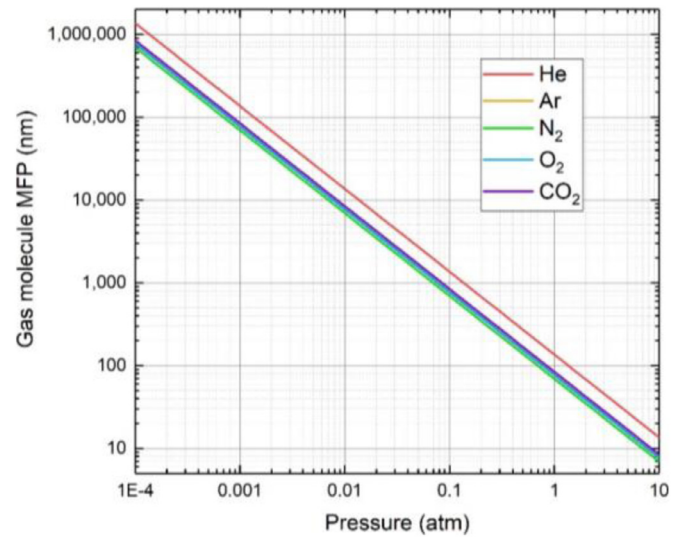


Fig. 6. Kinetic mean free paths (MFP) of He, Ar, N<sub>2</sub>, O<sub>2</sub>, and CO<sub>2</sub> gas molecules as a function of pressure at 300 K.

mal conductivity of gases. To have a general sense of the subcontinuum heat transfer regime, we first plot  $\Lambda$  as a function of pressure in Fig. 6 for He, Ar, N<sub>2</sub>, O<sub>2</sub>, and CO<sub>2</sub> at room temperature (300 K). At atmospheric pressure (1 atm),  $\Lambda$  of these gases ranges from 69 to 136 nm, indicating that  $\kappa_{gas}$  can experience a size effect (or subcontinuum heat transfer effect) at atmospheric pressure when the pore size is below a few hundred nanometers. At 0.001 atm,  $\Lambda$  increases to 69–136  $\mu\text{m}$ , and the size effect starts at a few hundred micrometers, which makes manufacturing of porous insulation materials more feasible since the pore sizes do not have to be as small.

The gas thermal conductivities as a function of pore size at  $P=1, 10^{-1}, 10^{-2}, 10^{-3}, 10^{-4},$  and  $10^{-5}$  atm are shown in Fig. 7. Similarly, the gas thermal conductivities as a function of pressure at  $D=100, 10, 1, 0.3, 0.1,$  and  $0.01 \mu\text{m}$  are shown in Fig. 8. Either reducing the pore size or pressure is an efficient way to reduce the thermal conductivity. For example, at a pore diameter of 10 nm, which has been constructed experimentally [56] that is at ambient pressure, the gas thermal conductivities of He, Ar, N<sub>2</sub>, and O<sub>2</sub> are as low as  $9.7 \times 10^{-4}, 3.4 \times 10^{-4}, 7.3 \times 10^{-4},$  and  $8.5 \times 10^{-4}$  W•m<sup>-1</sup>•K<sup>-1</sup>, respectively, which are two to three orders of magnitude lower than their bulk values. Even for a larger pore size (e.g., 100 nm) at ambient pressure, the thermal conductivity of He, Ar, N<sub>2</sub>, and O<sub>2</sub> are  $9.0 \times 10^{-3}, 2.8 \times 10^{-3}, 5.7 \times 10^{-3},$  and  $6.5 \times 10^{-3}$

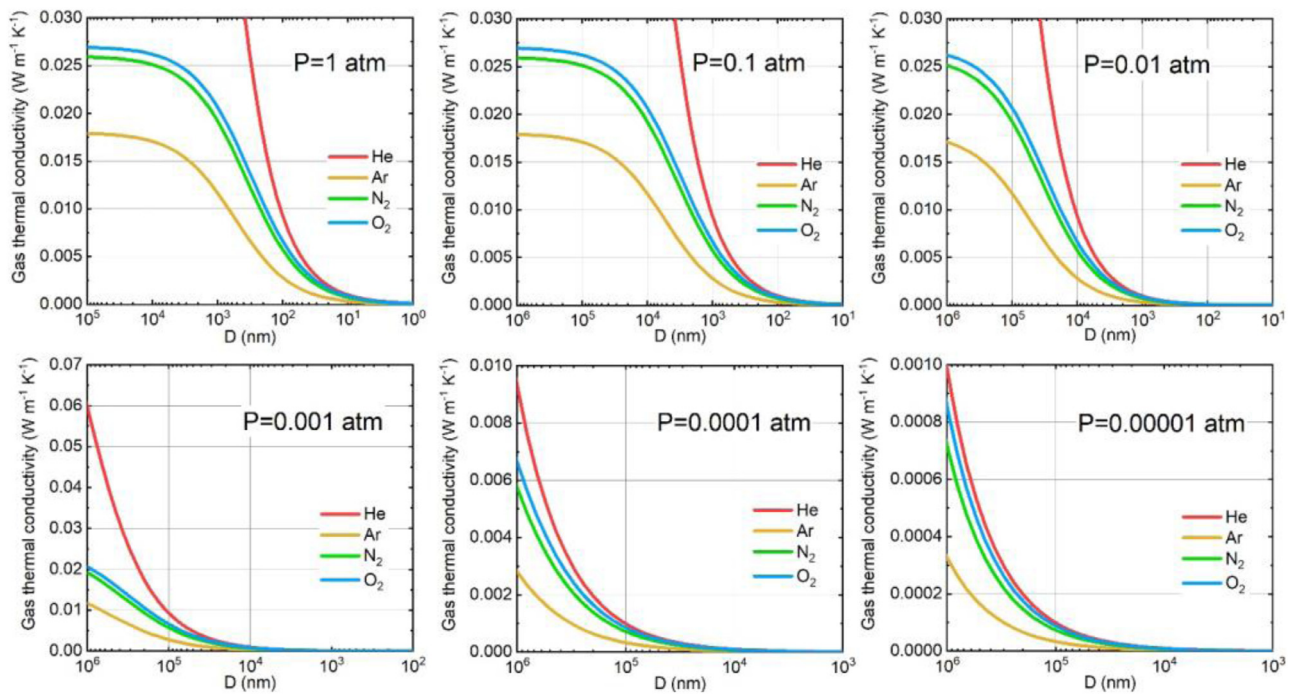


Fig. 7. Gas thermal conductivities of He, Ar, N<sub>2</sub>, and O<sub>2</sub> as a function of pore diameter (*D*) at various pressures at 300 K.

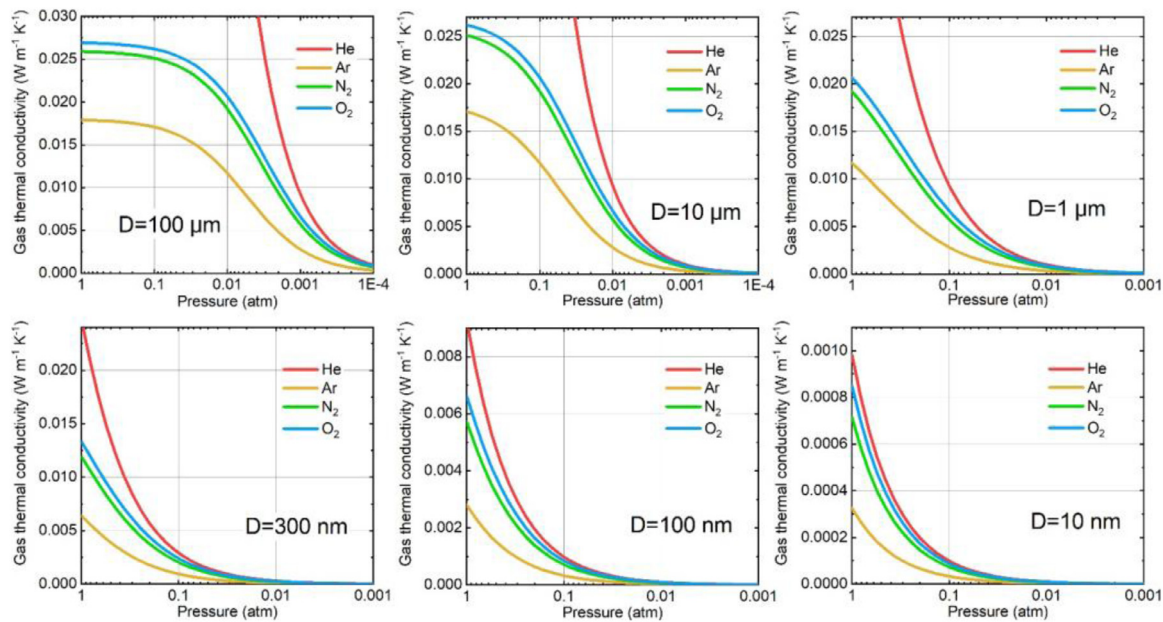


Fig. 8. Gas thermal conductivities of He, Ar, N<sub>2</sub>, and O<sub>2</sub> as a function of pressure for different pore diameters (*D*) at 300 K.

$W \cdot m^{-1} \cdot K^{-1}$ , respectively, which are still several times lower than their bulk values. These extremely low thermal conductivity values are nearly negligible when compared to other heat transfer components, such as solid conduction and radiation, in typical thermal insulation materials. Because gas conduction often makes the greatest contribution to the thermal conductivity of porous thermal insulation materials, reducing it will improve thermal performance. Figs. 7 and 8 provide a general guideline for the design of porous materials with low thermal conductivities.

To examine the effect of the accommodation coefficient on gas thermal conductivity at various pore sizes and pressures, in Fig. 9 we compare the thermal conductivities of the studied gases using their  $\alpha$  (or  $\beta$ ) values obtained in this work with those typically

used in the literature (i.e.,  $\alpha = 1$ ,  $\beta = 1.5$ ). The effect of the accommodation coefficient increases considerably as the pore size or pressure is reduced. For example, when the pore size is 10 nm and at atmospheric pressure, the accommodation coefficients obtained in this work can reduce the thermal conductivity values by 72%, 55%, 40%, and 25% for He, Ar, N<sub>2</sub>, and O<sub>2</sub>, respectively. Even if the pore size is 100 nm, a more practical value for manufacturing, such reductions can be as large as 68%, 47%, 33%, and 20%, respectively. Therefore, the correct accommodation coefficient could be key in designing ultra-low thermal conductivity insulation materials.

To estimate the influence of accommodation coefficients on the effective thermal conductivity of thermal insulation materials, we assume a thermal insulation material made of porous polystyrene

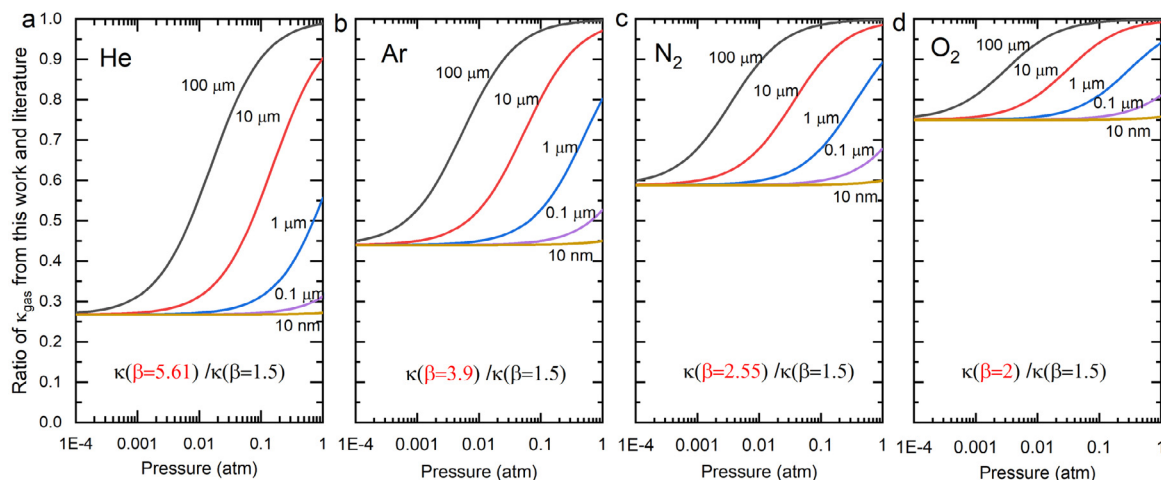


**Fig. 9.** Ratio of gas thermal conductivities that are calculated using the  $\beta$  values obtained in this work (red values in the graphs) and those typically used in the literature (i.e.,  $\alpha = 1$ , or  $\beta = 1.5$ ). (a) He, (b) Ar, (c)  $N_2$ , and (d)  $O_2$ . For each gas, several pore sizes are shown. (For interpretation of the colors in this figure legend, the reader is referred to the web version of this article.)

with a porosity of  $\phi = 95\%$  and 100 nm pores that are filled with air at 1 atm. The solid thermal conductivity estimated by the effective medium approximation [57, 58] is about  $\kappa_{solid} = \frac{1-\phi}{1+\phi/2} \kappa_0 = 5.1 \times 10^{-3} \text{ W}\cdot\text{m}^{-1}\cdot\text{K}^{-1}$ , where  $\kappa_0 = 0.15 \text{ W}\cdot\text{m}^{-1}\cdot\text{K}^{-1}$  is the thermal conductivity of bulk polystyrene. The gas thermal conductivity  $\kappa_{gas}$  based on Eq. (7) using the commonly accepted  $\beta$  value of 1.5 vs. the one obtained in this work are  $8.3 \times 10^{-3}$  and  $5.8 \times 10^{-3} \text{ W}\cdot\text{m}^{-1}\cdot\text{K}^{-1}$ , respectively. Ignoring the radiation contribution, the accommodation coefficient obtained in this work reduces the effective thermal conductivity  $\kappa_{solid} + \kappa_{gas}$  from  $13.4 \times 10^{-3}$  to  $10.9 \times 10^{-3} \text{ W}\cdot\text{m}^{-1}\cdot\text{K}^{-1}$  or by 19%. These results may serve as an incentive to manufactures of extruded polystyrene foams to attempt to decrease their pore sizes. Next steps for this research include validating the simulation results through experimentation.

Aside from the gases discussed above, we also considered  $CO_2$ . Although we do not have a conclusive result for  $CO_2$  due to the large fluctuation in the MD simulations, it is plausible that its accommodation coefficient is close to 1 due to its heavy mass and strong interaction with polymers.

## 8. Conclusions

In conclusion, by using NEMD simulations, we reveal the energy accommodation coefficients for He, Ar,  $N_2$ , and  $O_2$  on polymer surfaces. We find that their values range from 0.5 to 0.9, depending on the interaction strength between the gas and the polymer. The accommodation coefficient for air with polystyrene is about 0.81, which is validated by our experimentally measured pressure-dependent thermal conductivity of expanded polystyrene filled with air. Compared with the commonly assumed value of 1, the energy accommodation coefficients revealed in this work can significantly reduce gas thermal conductivity when the pore size is small ( $< \mu\text{m}$ ) or the pressure is low ( $< 0.1 \text{ atm}$ ). Such reduction can be up to 72%, 55%, 40%, and 25% for He, Ar,  $N_2$ , and  $O_2$ , respectively. These findings are critical to developing ultra-low thermal conductivity-insulation materials. With the revised accommodation coefficients, one can precisely design the pore size of foams and the pressure used in the foams to reach a specific thermal conductivity target. The low accommodation coefficient of He suggests that it has the potential to be a promising choice for thermal insulation at low pressure despite its high bulk thermal conductivity. In the future, we expect to conduct more simulations and experiments to reveal the energy accommodation coefficients between more complex gases, e.g., pentane, and polymers. These studies

will benefit the development of thermal insulation materials for broad applications such as oil transportation, aerospace engineering, and building envelopes.

## Author contributions

T.F. conducted the simulations and wrote the manuscript. S.S.S identified the knowledge gap. S.S.S and D.H. secured funds from DOE and guided the project. S.S.S., D.H., and A.R. contributed to discussion and manuscript revision.

## Additional note from the US Department of energy (DOE)

*This manuscript has been authored by UT-Battelle, LLC, under contract DE-AC05-00OR22725 with the US Department of Energy (DOE). The US Government retains and the publisher, by accepting the article for publication, acknowledges that the US government retains a nonexclusive, paid-up, irrevocable, worldwide license to publish or reproduce the published form of this manuscript, or allow others to do so, for US government purposes. DOE will provide public access to these results of federally sponsored research in accordance with the DOE Public Access Plan (<http://energy.gov/downloads/doe-public-access-plan>).*

## Declaration of Competing Interest

The authors declare no conflicts of interest. The funders had no role in the design of the study; in the collection, analyses, or interpretation of data; in the writing of the manuscript; or in the decision to publish the results.

## CRediT authorship contribution statement

**Tianli Feng:** Conceptualization, Data curation, Formal analysis, Investigation, Methodology, Validation, Writing - original draft. **Amit Rai:** Validation, Writing - review & editing. **Diana Hun:** Funding acquisition, Supervision, Project administration, Resources, Writing - review & editing. **Som S Shrestha:** Conceptualization, Funding acquisition, Supervision, Resources, Writing - review & editing.

## Acknowledgment

This work is supported by the project "Models to Evaluate and Guide the Development of Low Thermal Conductivity Materials for

Building Envelopes" funded by Building Technologies Office (BTO), Office of Energy Efficiency & Renewable Energy (EERE) at the Department of Energy (DOE). Computations were performed at the National Energy Research Scientific Computing Center (NERSC), the Compute and Data Environment for Science (CADES) at Oak Ridge National Laboratory (ORNL), and the Extreme Science and Engineering Discovery Environment (XSEDE).

## References

- [1] A. Korjenic, V. Petráněk, J. Zach, J. Hroudová, Development and performance evaluation of natural thermal-insulation materials composed of renewable resources, *Energy Build.* 43 (2011) 2518–2523 <https://doi.org/10.1016/j.enbuild.2011.06.012>.
- [2] S. Shrestha, A. Rai, T. Feng, M. Zhang, D.E. Hun, K. Biswas, A.O. Desjarlais, Review of models to evaluate and guide the development of low-thermal-conductivity materials, in: *Therm. Perform. Extrem. Envel. Whole Build. XIV Int. Conf.* (2019) 67 [https://www.techstreet.com/standards/review-of-models-to-evaluate-and-guide-the-development-of-low-thermal-conductivity-materials?product\\_id=2095251#jumps](https://www.techstreet.com/standards/review-of-models-to-evaluate-and-guide-the-development-of-low-thermal-conductivity-materials?product_id=2095251#jumps).
- [3] U.S. energy information administration / monthly energy review march 2020, (2020) 37. [https://www.eia.gov/totalenergy/data/monthly/pdf/sec2\\_3.pdf](https://www.eia.gov/totalenergy/data/monthly/pdf/sec2_3.pdf).
- [4] A.G. Gaglia, E.N. Dyalynas, A.A. Argiriou, E. Kostopoulou, D. Tsiamitros, D. Stimoniaris, K.M. Laskos, Energy performance of European residential buildings: energy use, technical and environmental characteristics of the Greek residential sector – energy conservation and CO<sub>2</sub> reduction, *Energy Build.* 183 (2019) 86–104 <https://doi.org/10.1016/j.enbuild.2018.10.042>.
- [5] Residential energy consumption survey (RECS), (2015). <https://www.eia.gov/consumption/residential/index.php>.
- [6] A.M. Papadopoulos, State of the art in thermal insulation materials and aims for future developments, *Energy Build.* 37 (2005) 77–86 <https://doi.org/10.1016/j.enbuild.2004.05.006>.
- [7] D.M.S. Al-Homoud, Performance characteristics and practical applications of common building thermal insulation materials, *Build. Environ.* 40 (2005) 353–366 <https://doi.org/10.1016/j.buildenv.2004.05.013>.
- [8] L. Braginsky, V. Shklover, G. Witz, H.-P. Bossmann, Thermal conductivity of porous structures, *Phys. Rev. B.* 75 (2007) 094301 <https://doi.org/10.1103/PhysRevB.75.094301>.
- [9] M. Obori, D. Suh, S. Yamasaki, T. Kodama, T. Saito, A. Isogai, J. Shiomi, Parametric model to analyze the components of the thermal conductivity of a cellulose-nanofibril aerogel, *Phys. Rev. Appl.* 11 (2019) 024044 <https://doi.org/10.1103/PhysRevApplied.11.024044>.
- [10] B.P. Jelle, Traditional, state-of-the-art and future thermal building insulation materials and solutions – properties, requirements and possibilities, *Energy Build.* 43 (2011) 2549–2563 <https://doi.org/10.1016/j.enbuild.2011.05.015>.
- [11] S.Q. Zeng, A. Hunt, R. Greif, Mean free path and apparent thermal conductivity of a gas in a porous medium, *J. Heat Transf.* 117 (1995) 758 <https://doi.org/10.1115/1.2822642>.
- [12] C. Bi, G.H. Tang, Effective thermal conductivity of the solid backbone of aerogel, *Int. J. Heat Mass Transf.* 64 (2013) 452–456 <https://doi.org/10.1016/j.ijheatmasstransfer.2013.04.053>.
- [13] E. Litovsky, M. Shapiro, A. Shavit, Gas pressure and temperature dependences of thermal conductivity of porous ceramic materials: part 2, refractories and ceramics with porosity exceeding 30%, *J. Am. Ceram. Soc.* 79 (1996) 1366–1376 <https://doi.org/10.1111/j.1151-2916.1996.tb08598.x>.
- [14] S.N. Schiffres, K.H. Kim, L. Hu, A.J.H. McGaughey, M.F. Islam, J.A. Malen, Gas diffusion, energy transport, and thermal accommodation in single-walled carbon nanotube aerogels, *Adv. Funct. Mater.* 22 (2012) 5251–5258 <https://doi.org/10.1002/adfm.201201285>.
- [15] Z. Liang, W. Evans, T. Desai, P. Keblinski, Improvement of heat transfer efficiency at solid-gas interfaces by self-assembled monolayers, *Appl. Phys. Lett.* (2013) 102 <https://doi.org/10.1063/1.4792530>.
- [16] Y. Xiong, X. Yu, Y. Huang, J. Yang, L. Li, N. Yang, D. Xu, Ultralow thermal conductance of the van der Waals interface between organic nanoribbons, *Mater. Today Phys.* (2019) 11 <https://doi.org/10.1016/j.mtphys.2019.100139>.
- [17] R. Ma, X. Wan, T. Zhang, N. Yang, T. Luo, Role of molecular polarity in thermal transport of boron nitride-organic molecule composites, *ACS Omega* 3 (2018) 12530–12534 <https://doi.org/10.1021/acsomega.8b02338>.
- [18] D. Singh, X. Guo, A. Alexeenko, J.Y. Murthy, T.S. Fisher, Modeling of subcontinuum thermal transport across semiconductor-gas interfaces, *J. Appl. Phys.* 106 (2009) 1–13 <https://doi.org/10.1063/1.3181059>.
- [19] C. Cheng, W. Fan, J. Cao, S.G. Ryu, J. Li, C.P. Grigoropoulos, J. Wu, Heat transfer across the interface between nanoscale solids and gas, *ACS Nano* 5 (2011) 10102–10107 <https://doi.org/10.1021/nn204072n>.
- [20] Z. Liang, W. Evans, P. Keblinski, Equilibrium and nonequilibrium molecular dynamics simulations of thermal conductance at solid-gas interfaces, *Phys. Rev. E - Stat. Nonlinear, Soft Matter Phys.* 87 (2013) 3–9 <https://doi.org/10.1103/PhysRevE.87.022119>.
- [21] F.O. Goodman, *J. Phys.* Thermal accommodation coefficients, *Chem* 84 (1980) 1431–1445 <https://doi.org/10.1021/j100449a002>.
- [22] S.C. Saxena, S.H.P. Chen, Thermal accommodation coefficients for the gas-saturated tungsten-nitrogen and tungsten-carbon dioxide systems, *J. Phys. B At. Mol. Phys.* 10 (1977) 2011–2022 <https://doi.org/10.1088/0022-3700/10/10/030>.
- [23] J.R. Wolf, W.C. Strieder, Pressure-dependent gas heat transport in a spherical pore, *AIChE J* 40 (1994) 1287–1296 <https://doi.org/10.1002/aic.690400803>.
- [24] L. Hu, A.J.H. McGaughey, Energy accommodation between noble gases and carbon nanotubes, *J. Phys. Chem. C* 117 (2013) 18804–18808 <https://doi.org/10.1021/jp404153d>.
- [25] K.J. Daun, G.J. Smallwood, F. Liu, Molecular dynamics simulations of translational thermal accommodation coefficients for time-resolved LII, *Appl. Phys. B Lasers Opt.* 94 (2009) 39–49 <https://doi.org/10.1007/s00340-008-3277-y>.
- [26] W.M. Trott, J.N. Castaeda, J.R. Torczynski, M.A. Gallis, D.J. Rader, An experimental assembly for precise measurement of thermal accommodation coefficients, *Rev. Sci. Instrum.* (2011) 82 <https://doi.org/10.1063/1.3571269>.
- [27] W.O. Ho, Measurement of thermal accommodation coefficients of steel surfaces, *Univ. Mo. - Roll A* (1970).
- [28] G. Reichenauer, U. Heinemann, H.P. Ebert, Relationship between pore size and the gas pressure dependence of the gaseous thermal conductivity, *Colloids Surf. A Physicochem. Eng. Asp.* 300 (2007) 204–210 <https://doi.org/10.1016/j.colsurfa.2007.01.020>.
- [29] M.A. Gallis, D.J. Rader, J.R. Torczynski, Thermophoresis in rarefied gas flows, *Aerosol Sci. Technol.* 36 (2002) 1099–1117 <https://doi.org/10.1080/02786820290092168>.
- [30] J. Fricke, H. Schwab, U. Heinemann, Vacuum insulation panels - exciting thermal properties and most challenging applications, *Int. J. Thermophys.* 27 (2006) 1123–1139 <https://doi.org/10.1007/s10765-006-0106-6>.
- [31] R. Coquard, D. Baillis, V. Grigorova, F. Enguehard, D. Quenard, P. Levitz, Modelling of the conductive heat transfer through nano-structured porous silica materials, *J. Non. Cryst. Solids* 363 (2013) 103–115 <https://doi.org/10.1016/j.jnoncrysol.2012.11.053>.
- [32] J.S. Kwon, C.H. Jang, H. Jung, T.H. Song, Effective thermal conductivity of various filling materials for vacuum insulation panels, *Int. J. Heat Mass Transf.* 52 (2009) 5525–5532 <https://doi.org/10.1016/j.ijheatmasstransfer.2009.06.029>.
- [33] U. Heinemann, R. Caps, J. Fricke, Radiation-conduction interaction: an investigation on silica aerogels, *Int. J. Heat Mass Transf.* 39 (1996) 2115–2130 [https://doi.org/10.1016/0017-9310\(95\)00313-4](https://doi.org/10.1016/0017-9310(95)00313-4).
- [34] K. Raed, U. Gross, Modeling of influence of gas atmosphere and pore-size distribution on the effective thermal conductivity of knudsen and non-knudsen porous materials, *Int. J. Thermophys* 30 (2009) 1343–1356 <https://doi.org/10.1007/s10765-009-0600-8>.
- [35] F.O. Goodman, H.Y. Wachman, Dynamics of Gas-Surface Scattering, Elsevier, 1976 <https://doi.org/10.1016/B978-0-12-290450-9.X5001-5>.
- [36] G.S. Hwang, M. Kaviany, Molecular dynamics simulation of effective thermal conductivity of vapor-filled nanogap and nanocavity, *J. Appl. Phys.* 106 (2009) 024317 <https://doi.org/10.1063/1.3186043>.
- [37] S. Plimpton, Fast parallel algorithms for short-range molecular dynamics, *J. Comput. Phys.* 117 (1995) 1–19.
- [38] See <http://accelrys.com/products/materials-studio/> for "Accelrys Software, Inc., Materials Studio v 7.0." (n.d.).
- [39] X. Wei, T. Luo, Chain length effect on thermal transport in amorphous polymers and a structure-thermal conductivity relation, *Phys. Chem. Chem. Phys.* 21 (2019) 15523–15530 <https://doi.org/10.1039/c9cp02397f>.
- [40] J. Zhao, J.W. Jiang, N. Wei, Y. Zhang, T. Rabczuk, Thermal conductivity dependence on chain length in amorphous polymers, *J. Appl. Phys.* (2013) 113 <https://doi.org/10.1063/1.4804237>.
- [41] M.-J. Huang, C.-C. Weng, T.-M. Chang, An investigation of the phonon properties of silicon nanowires, *Int. J. Therm. Sci.* 49 (2010) 1095–1102 <https://doi.org/10.1016/j.ijthermalsci.2010.02.002>.
- [42] A. Bagri, S. Kim, R. Ruoff, V. Shenoy, Thermal transport across twin grain boundaries in polycrystalline graphene from nonequilibrium molecular dynamics simulations, *Nano Lett.* 11 (2011) 3917–3921 <http://pubs.acs.org/doi/abs/10.1021/nl202118d>. (accessed August 16, 2013).
- [43] X. Lu, X. Chen, Y.S. Wang, Y.Y. Tan, Z.Y. Gaomu, Molecular dynamics simulation of gas transport in amorphous polypropylene, *Wuli Huaxue Xuebao/Acta Phys. - Chim. Sin.* 32 (2016) 2523–2530 <https://doi.org/10.3866/PKU.WHXB201606292>.
- [44] D. Dubbeldam, H. Frost, K.S. Walton, R.Q. Snurr, Molecular simulation of adsorption sites of light gases in the metal-organic framework IRMOF-1, *Fluid Phase Equilib* 261 (2007) 152–161 <https://doi.org/10.1016/j.fluid.2007.07.042>.
- [45] R.E. Tuzun, D.W. Noid, B.G. Sumpter, R.C. Merkle, Dynamics of fluid flow inside carbon nanotubes, *Nanotechnology* 7 (1996) 241–246 <https://doi.org/10.1088/0957-4484/7/3/012>.
- [46] M.P. Allen, D.J. Tildesley, *Computer Simulation of Liquids*, Oxford university, New York, 1987.
- [47] H.Y. WACHMAN, The thermal accommodation coefficient: a critical survey, *ARS J.* 32 (1962) 2–12 <https://doi.org/10.2514/8.5939>.
- [48] A.T. Rosenberger, E.B. Dale, D. Ganta, J.P. Rezac, Investigating properties of surfaces and thin films using microsphere whispering-gallery modes, *Laser Res. Beam Control A* 6872 (2008) 68720U <https://doi.org/10.1117/1.2.772655>.
- [49] F.O. Goodman, H.Y. Wachman, Formula for thermal accommodation coefficient, 1966.
- [50] M. Grau, F. Völklein, A. Meier, C. Kunz, J. Heidler, P. Woias, Method for measuring thermal accommodation coefficients of gases on thin film surfaces using a MEMS sensor structure, *J. Vac. Sci. Technol. A Vac., Surf. Film* 34 (2016) 041601 <https://doi.org/10.1116/1.4948527>.
- [51] M.G. Kaganer, *Thermal insulation in cryogenic engineering*, Jerus. Isr. Prog. Sci. Transl. (1969).
- [52] Thermal conductivity of gases chart, *Heat Transf. Eng. Des.* (n.d.). [https://www.engineersedge.com/heat\\_transfer/thermal-conductivity-gases.htm](https://www.engineersedge.com/heat_transfer/thermal-conductivity-gases.htm).

- [53] S. Matteucci, Y. Yampolskii, B.D. Freeman, I. Pinnau, Transport of gases and vapors in glassy and rubbery polymers, *Mater. Sci. Membr. Gas Vap. Sep.* 1 (2006) 1–2.
- [54] D.W. Breck, *Zeolite molecular sieves: structure, chemistry and use*, Krieger (1984).
- [55] A.F. Ismail, K.C. Khulbe, T. Matsuura, *Gas Separation Membranes*, Springer, Switz, 2015.
- [56] D. Wu, C.M. Hui, H. Dong, J. Pietrasik, H.J. Ryu, Z. Li, M. Zhong, H. He, E.K. Kim, M. Jaroniec, T. Kowalewski, K. Matyjaszewski, Nanoporous polystyrene and carbon materials with core-shell nanosphere-interconnected network structure, *Macromolecules* 44 (2011) 5846–5849 <https://doi.org/10.1021/ma2013207>.
- [57] J.C. Maxwell, *A Treatise on Electricity and Magnetism*, Clarendon press, 1881.
- [58] A. Eucken, Allgemeine gesetzmäßigkeiten für das wärmeleitvermögen verschiedener stoffarten und aggregatzustände, *Forsch. Auf. Dem. Gebiet Des. Ingenieurwesens A.* 11 (1940) 6–20.
- [59] H. W. Russell, PRINCIPLES OF HEAT FLOW IN POROUS INSULATORS, *Journal of the American Ceramic Society* 18 (1935) 1–5, doi:10.1111/j.1151-2916.1935.tb19340.x.